

# A new strategy for accurate targeted diagnosis and treatment of cutaneous malignant melanoma: dual-mode phase-change lipid nanodroplets as ultrasound contrast agents

This article was published in the following Dove Press journal:  
*International Journal of Nanomedicine*

Hengli Yang<sup>1,2,\*</sup>  
Wenbin Cai<sup>3,\*</sup>  
Wei Lv<sup>2</sup>  
Ping Zhao<sup>2</sup>  
Yamei Shen<sup>4</sup>  
Longfang Zhang<sup>1</sup>  
Bin Ma<sup>1</sup>  
Lijun Yuan<sup>2</sup>  
Yunyou Duan<sup>2</sup>  
Kechun Yao<sup>1</sup>

<sup>1</sup>Department of Ultrasound Diagnosis, Air Force General Hospital, Beijing, People's Republic of China; <sup>2</sup>Department of Ultrasound Diagnosis, Tang Du Hospital, Fourth Military Medical University, Xi'an, People's Republic of China; <sup>3</sup>Special Diagnosis Department, General Hospital of Tibet Military Command, Lhasa, People's Republic of China; <sup>4</sup>Department of Ultrasound Diagnosis, Shaanxi Provincial People's Hospital, Xi'an, People's Republic of China

\*These authors contributed equally to this work

**Background:** Currently, effective detection and treatment of cutaneous malignant melanoma (CMM) still face severe challenges. Ultrasound molecular imaging as a noninvasive and easy-to-operate method is expected to bring improvements for tumor detection.

**Purpose:** The aim of this research is to prepare novel phase-change ultrasound contrast agents, Nds-IR780, which can perform not only dual-mode molecule-targeted imaging but also targeted photothermal therapy for CMM.

**Methods:** A double emulsion process was used to prepare the Nds-IR780. Then, the entrapment rate and drug loading of IR-780 iodide in Nds-IR780 were detected by high-performance liquid chromatography. The biocompatibility of Nds-IR780 was evaluated by a CCK-8 assay and the characteristics and stability of that were verified through the particle size analyzer, laser scanning confocal microscopy (LSCM) and transmission electron microscopy (TEM). The abilities of dual-mode molecule-targeted imaging and targeted photothermal therapy for Nds-IR780 were confirmed via the in vitro and in vivo experiments.

**Results:** Nds-IR780 had good size distribution, polydispersity index, stability and biosafety. The in vitro and in vivo experiments confirmed that Nds-IR780 were capable of targeting CMM cells with high affinity (22.4±3.2%) and facilitating dual-mode imaging to detect the primary lesion and sentinel lymph nodes (SLNs) of CMM. Furthermore, the photothermal ablation of CMM mediated by Nds-IR780 was very effective in vivo.

**Conclusion:** The newly prepared Nds-IR780 were observed to be effective targeted therapeutic probe for the precise detection and targeted treatment of CMM.

**Keywords:** CMM, dual-mode phase-change nanodroplets, targeted accurate diagnosis and treatment

## Introduction

Cutaneous malignant melanoma (CMM) is a highly aggressive malignant tumor of the skin.<sup>1-3</sup> Although the incidence of this disease is not high, the prognosis is extremely poor because of its high malignancy, early metastasis to the lymphatic and hematic tracts and insensitivity to radiotherapy and chemotherapy.<sup>4</sup> Recently, it has been confirmed that the incidence of CMM is increasing year by year, and its development speed has far exceeded that of other malignant tumors.<sup>5</sup> Currently, despite improvements to the overall survival, staging, classification and treatment of CMM,<sup>1</sup> there remains a challenge in the accurate assessment of small melanomas that may have metastatic potential.<sup>2</sup> Moreover, there are overlapping histopathological features between some CMMs and certain types of skin

Correspondence: Yunyou Duan  
Department of Ultrasound Diagnosis,  
Tang Du Hospital, Fourth Military Medical  
University, Xi'an 710038, People's  
Republic of China  
Email duanyy@fmmu.edu.cn

Kechun Yao  
Department of Ultrasound Diagnosis, Air  
Force General Hospital, Beijing 100036,  
People's Republic of China  
Email yaokc1959@hotmail.com

abnormalities, making the identification between benign and malignant tumors difficult through histopathological examination.<sup>6</sup> Given these challenges, it is urgent to explore an accurate assessment strategy to precisely detect cutaneous malignant melanoma and even to perform effective treatment.

Recently, molecular targeting imaging technologies have been developed, such as MRI, SPECT and PET,<sup>7</sup> and these imaging modalities are expected to bring about precise detection of small primary lesions, sentinel lymph nodes (SLNs) and metastases by imaging specific molecules of the tumors; some have already been applied to the clinic. However, the disadvantages of radioactive contamination and high cost limit these imaging modalities from wide application in the clinic. Molecular targeted contrast-enhanced ultrasound imaging is a new technology that has been developed in recent years. Compared with MRI, SPECT or PET, ultrasound has many advantages including no radiation, real-time display, simple operation, and low cost. Usually, a good ultrasound contrast agent is the key to the implementation of molecular targeted contrast-enhanced ultrasound imaging. In past decades, microbubbles carrying specific targeting antibodies, drugs or genes have been used as ultrasound contrast agents for targeted intravascular diagnosis and treatment for tumors or inflammation, which has been widely studied.<sup>8</sup> However, the large particle size of microbubbles limits their penetration into the tumor vascular endothelial gap (380–780 nm) to target the majority of the molecules that exist in tumor cells. Therefore, to achieve targeted extravascular ultrasound molecular imaging, nano-sized ultrasound contrast agents are urgently needed.

In recent years, phase-change nanoscale droplets as ultrasound contrast agents have been developed. The phase-change nanodroplets have a suitable particle size and can extravasate out of the tumor vasculature and accumulate in the tumor interstitium through the enhanced permeability and retention (EPR) effect. Then, under sufficient negative pressure, the nanodroplets can be vaporized into microbubbles; the procedure is often referred to as acoustic droplet vaporization.<sup>9</sup> After the phase transition, the microbubbles that accumulated in the tumor interstitium can realize precise ultrasound imaging and targeted treatment for tumors. Compared with microbubbles as ultrasound contrast agents, phase-change nanodroplets not only arrive at the specific tumor molecules but also retain a long circulation half-time in vivo.<sup>10,11</sup> However, research on phase-change nanodroplets for accurate diagnosis and targeted treatment of tumors is still in its infancy.

Liming Deng et al<sup>12</sup> prepared multimodal nanoparticles encapsulating a perfluoropentane (PFP) liquid core to realize magnetic resonance (MR)/photoacoustic (PA)/ultrasound (US)/near-infrared fluorescence (NIRF) multimodal imaging and photothermal therapy (PTT) for breast cancer. To date, there are no reports on using phase-change nanodroplets as ultrasound contrast agents to precisely detect CMM.

In this study, we prepared novel bimodal theranostic phase-change nanodroplets named Nds-IR780 for the precise detection and targeted treatment of CMM (Figure 1). IR-780 iodide, a near infrared fluorescence (NIRF) dye, can not only be used for near infrared fluorescence imaging but can also effectively target tumors by identifying organic-anion transporting polypeptides (OATPs), which are usually overexpressed in tumor cells.<sup>13–15</sup> Furthermore, IR-780 iodide can be a thermosensitive agent that mediates heat ablation therapy in tumors. However, IR-780 iodide is difficult to dissolve in water, and this disadvantage greatly restricts its application in the clinic. In recent studies, IR-780 iodide has mainly been carried on nanoparticles to achieve the desired results. However, some concerns about the safety of nanoparticle metabolism still exist. Nanodroplets, with their liposoluble characteristics, carried the IR-780 iodide on the lipid surface in our study. The newly prepared Nds-IR780 had good physical and chemical properties, and its potential application value for accurate detection and targeted heat ablation for primary CMM and SLNs was confirmed.

## Materials and methods

### Materials

Liquid fluorocarbon perfluorohexane (PFH) was purchased from Xi'an ruixi Biological Technology Co., Ltd. High purity 1,2-dipalmitoyl-sn-glycero-3-phosphocholine (DPPC) and 1,2-distearoyl-sn-glycero-3-phosphoethanolamine-N-[polyethylene glycol-2000] (DSPE-PEG2000), the main components of the Nds film, were purchased in powder form (Avanti Polar Lipids Inc., Alabaster, AL, USA). IR-780 iodide was purchased from Sigma-Aldrich (St. Louis, MO, USA). Hoechst 33342 was purchased from Beyotime Technology (Shanghai, China), and chloroform was purchased from Kehao Co. Cell Counting Kit-8 (CCK-8) was obtained from Dojindo (Japan). All other chemical reagents were of analytical grade and were used as received without further purification.

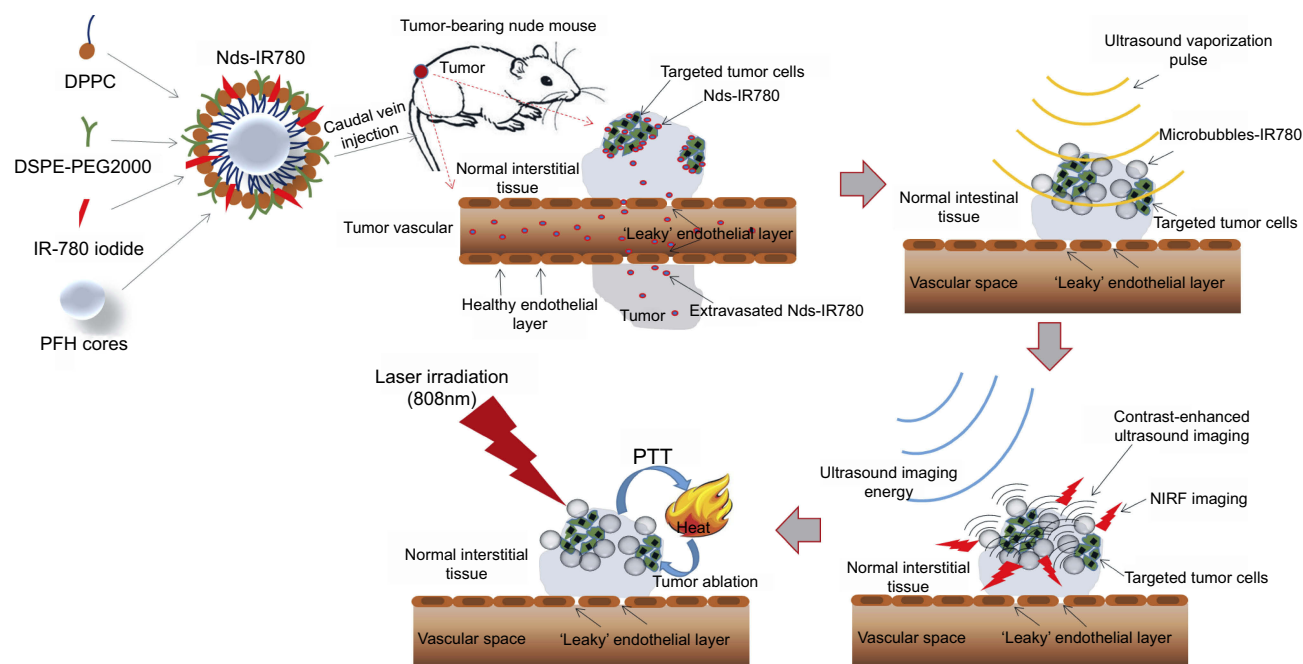


**Figure 1** The preparation scheme for Nds-IR780 and the diagram of dual-mode molecule-targeted imaging and photothermal therapy for tumors.

## Preparation of Nds-IR780

A double emulsion process was used to prepare the Nds-IR780 compound. First, three same hybrid lipid solution processes were prepared. A total of 14 mg of DPPC and DSPE-PEG2000 at an appropriate mass ratio was dissolved in 6 mL chloroform in a 50-mL flask. Then, 25  $\mu$ L, 50  $\mu$ L and 75  $\mu$ L IR-780 iodide (2 mg/mL) were added to the solution. The mixture was agitated lightly (5 min, 300 rpm) via a magnetic stirrer and rotary evaporated for 30 min at 55  $^{\circ}$ C and 135 rpm to obtain the dried thin film. Then, the film was hydrated with 5 mL hydration liquid (PBS: glycerol=9:1 (v/v)), and the lipid solution was performed using a high-speed dispersed homogenizer at 10,000 rpm for 5 min on ice. Then, the PFH was added drop by drop to the solution at a 1:8 proportion (PFH: lipid resolution). Finally, an ultrasonic homogenizer was used to emulsify the mixture for 130 s on ice. The samples were stored at 4  $^{\circ}$ C for the next experiments.

## The entrapment rate (ER) and drug loading (DL) of IR-780 iodide in Nds-IR780

The nanodroplets of the above three samples (with 50  $\mu$ g, 100  $\mu$ g and 150  $\mu$ g IR-780 iodide) were collected through centrifugal technology at low temperature. Using high-performance liquid chromatography (HPLC), the standard curve of IR-780 iodide was drawn, and the drug content in

the suspensions was detected. Next, the ER and DL were calculated by Equations (1) and (2) as follows:

$$ER = \frac{\text{Mass of total IR - 780} - \text{Mass of untrapped IR - 780}}{\text{Mass of total IR - 780}} \times 100\% \quad (1)$$

$$DL = \frac{\text{Mass of total IR - 780} - \text{Mass of untrapped IR - 780}}{\text{Mass of total liposomes}} \times 100\% \quad (2)$$

## Biocompatibility of Nds-IR780

All types of tumor cells in this research were purchased from ATCC. The CMM cells SK-MEL-28 were selected to evaluate the cytotoxicity of Nds-IR780 in vitro through a Cell Counter Kit-8 (CCK-8) assay. First, SK-MEL-28 cells were incubated in 96-well plates at a density of 5000 cells per well and cultured with MEM media in a humidified atmosphere with 5% CO<sub>2</sub> at 37  $^{\circ}$ C. After 24 h, the culture media was substituted with the same volume of fresh MEM media containing various diluted concentrations of Nds-IR780 (an initial addition of 150  $\mu$ g IR-780 iodide and dilutions of 60 $\times$ , 50 $\times$ , 40 $\times$ , 30 $\times$ , 20 $\times$ , 10 $\times$ , and 5 $\times$ ) for 24 h. Each single concentration was repeated in five wells. Next, 10  $\mu$ L of the CCK-8 reagent was added to each well and incubated for 4 h. Lastly, the absorbance of each well was measured at 450 nm by an Infinite F200 multimode plate reader (Tecan, Männedorf, Switzerland). The cell survival rates at various concentrations of Nds-IR780 were calculated via the formula  $C = (A - A_0)/(A_1 - A_0)$

$\times 100\%$  (where C: the cell survival rate; A: the absorbance of experimental wells; A0: the absorbance of blank wells; and A1: the absorbance of control wells).

## The characteristics of Nds-IR780

To observe the characteristics of Nds-IR780, the Nds-IR780 suspension (with an initial addition of 150  $\mu\text{g}$  IR-780 iodide) was diluted 20 times, and 2 mL of the suspension was placed in a particle size analyzer (DelsaNano, Beckman Coulter, USA) at 25 °C to analyze the size distribution and zeta potential. Then, a drop of the diluted Nds-IR780 suspension was placed on a slide glass and examined using laser scanning confocal microscopy (LSCM, Olympus Fv1000, Japan) with the 100 $\times$  oil-immersion objective lens. The exciting light was 633 nm, and the emitted light was 780 nm. Simultaneously, another drop of the Nds-IR780 suspension was observed by transmission electron microscopy (TEM, FEIT12, USA). The above experiments were repeated at least in triplicate.

## Stability of Nds-IR780

The previously mentioned diluted Nds-IR780 suspensions were collected and stored at 4 °C. At 0 h, 24 h, 72 h and 12 days, the appearance change was noted by taking a picture, and the change in size distribution was explored using a particle size analyzer (DelsaNano, Beckman Coulter, USA).

## NIRF imaging of Nds-IR780 in vitro

First, Nds-IR780 (with an initial addition of 150  $\mu\text{g}$  IR-780 iodide) were placed in 96-well plates according to high to low concentration gradients (diluted with 10 $\times$ , 20 $\times$ , 30 $\times$ , 40 $\times$ , 50 $\times$ , 60 $\times$ ). The PBS and blank well were set as the negative and blank controls. NIRF imaging was performed using an IVIS Lumina II imaging station (Caliper Life Sciences, Hopkinton, MA, USA) with 633 nm as the excitation wavelength and 780 nm as the emission wavelength.

## Phase transition and ultrasound contrast imaging of Nds-IR780 in vitro

First, a latex glove fingertip containing 10 mL degassed water was immersed in a water bath with an ultrasound transducer on one side. Then, 2 mL of the above Nds-IR780 (20 $\times$ ) solution was injected into the fingertip, and ultrasound contrast imaging was recorded by a Mylab Twice Ultrasound System (Esaote, Italy) in visualization

mode with a 7.5 MHz transducer. Afterwards, the fingertip containing Nds-IR780 was irradiated by low frequency ultrasound (20 s, 2.5  $\text{w}/\text{cm}^2$ , continuous irradiation). Then, the ultrasound contrast imaging was again examined, and the results were saved on the computer. Both before and after the phase change of Nds-IR780, a drop of solution was taken and set on a glass slide, and the morphological change of Nds-IR780 was observed through optical microscopy.

## Tumor-specific targeting of Nds-IR780 in vitro

SK-MEL-28 cells were grouped and cultured in confocal petri dishes with minimum Eagle's medium (MEM) containing 10% FBS and maintained in a humidified atmosphere of 5%  $\text{CO}_2$  at 37 °C; the medium was changed every 2–3 days. When the cells reached approximately 80% confluency on the bottom of the confocal petri dishes, the MEM media was discarded, and the cells were washed with sterile 1 $\times$ PBS. One culture dish containing cells was treated with 100  $\mu\text{L}$  ( $1.2 \times 10^7$  nanodroplets/mL) sterile Nds-IR780, and another was treated with 100  $\mu\text{L}$  sterile IR-780 iodide solution (150  $\mu\text{g}$  IR-780 iodide added to 100  $\mu\text{L}$  PBS). The third culture dish containing cells was treated with 100  $\mu\text{L}$  PBS as a negative control. The culture dishes were incubated at room temperature for 40 min and then washed lightly with 1 $\times$ PBS three times. Then, 1 mL (1 mg/mL) of Hoechst 33342 was added, and the culture dishes were incubated at 37 °C for 15 min. After being washed with 1 $\times$ PBS three times, the cells were observed under a LSCM (Carl Zeiss, Oberkochen, Germany). All of the above-mentioned procedures were repeated three times and carried out in the absence of light using aluminum foil.

## The absorption of IR-780 iodide in tumor cells

The absorption of IR-780 iodide in tumor cells was verified via flow cytometry (FCM). SK-MEL-28 cells were cultured in three 25 mL culture bottles as previously described. After the cells reached 70–80% confluency, the cells in the three culture bottles were washed with 1 $\times$ PBS as previously described. Then, 500  $\mu\text{L}$  of the Nds-IR780 solution ( $1.2 \times 10^7$  nanodroplets/mL), IR-780 iodide solution (150  $\mu\text{g}$  IR-780 iodide added to 100  $\mu\text{L}$  PBS) and PBS were added to the culture bottles. The cells were incubated at room temperature for 40 min and then washed lightly with 1 $\times$ PBS three times. Next, the cells

were digested with trypsin before being collected in sterile test tubes for FCM analysis. All of the above-mentioned experiments were repeated at least three times.

## Animal models

All of the nude BALB/c mice (approximately 16–20 g) were housed in accordance with the Guide for the Care and Use of Laboratory Animals adopted by the National Institutes of Health, and all procedures were approved by the Institutional Animal Care and Use Committee at the Air Force General Hospital. SK-MEL-28 cells were suspended in 200  $\mu\text{L}$  1 $\times$ PBS and subcutaneously injected into the flanks of nude mice ( $5\times 10^6$  cells per mouse). All subsequent in vivo experiments began when the tumors reached a diameter of 0.7–1.0 cm.

## The tumor-targeted effect of Nds-IR780 in vivo

The tumor-bearing nude mice were divided into three groups ( $n=3/\text{group}$ ) and injected with 200  $\mu\text{L}$  saline, IR-780 iodide and Nds-IR780 via caudal vein, respectively. After 6 h, the nude mice were anesthetized with isoflurane and placed in the darkroom of the IVIS Lumina II imaging station (Caliper Life Sciences, Hopkinton, MA, USA) for NIRF imaging. The excitation wavelength was 633 nm, and the emission wavelength was 780 nm.

## The biodistribution of Nds-IR780 in vivo

The tumor-bearing nude mice were divided into three groups ( $n=3/\text{group}$ ), and all nude mice were intravenously injected with 200  $\mu\text{L}$  Nds-IR780 ( $2.4\times 10^7$  nanodroplets/mL). After 1 h, 8 h and 24 h, the nude mice of groups 1, 2, and 3 were sacrificed, and the tumor, heart, liver, spleen, lung, kidneys, and muscle were collected for NIRF imaging via an IVIS Lumina II imaging station (Caliper Life Sciences, Hopkinton, MA, USA). The excitation wavelength was 633 nm, and the emission wavelength was 780 nm.

## Dual-mode detection for tumor and SLNs via Nds-IR780 in vivo

First, the tumor-bearing nude mouse was anesthetized through intraperitoneal injection using 100  $\mu\text{L}$  of 1% sodium pentobarbital and placed on a plate for imaging. Then, the ultrasound probe was placed on the tumor and groin using the 2-D and color Doppler imaging modes. Next, 200  $\mu\text{L}$  of the Nds-IR780 solution ( $2.4\times 10^7$  nanodroplets/mL) was injected into the mouse via the tail vein. After 1 h, the tumor was irradiated by

placing the low frequency ultrasound transducer (20 s, 2.5  $\text{w}/\text{cm}^2$ , continuous irradiation) on the tumor surface; contrast-enhanced ultrasound imaging was then performed with a Mylab Twice Ultrasound System (Esaote, Italy) with a 7.5 MHz transducer. The above data and images were stored for offline examination. After 8 h, the tumor-bearing mouse was anesthetized using isoflurane and NIRF imaging was performed via an IVIS Lumina II imaging station (Caliper Life Sciences, Hopkinton, MA, USA). All of the above experiments were repeated at least three times.

## Targeted photothermal therapy of Nds-IR780 in vivo

The tumor-bearing nude mice were divided into three groups ( $n=6/\text{group}$ ). Group 1, 2, and 3 were injected with Nds-IR780, IR-780 iodide and saline, respectively, through the caudal vein. First, all of the nude mice were anesthetized with 100  $\mu\text{L}$  of 1% sodium pentobarbital by intraperitoneal injection. Then, 200  $\mu\text{L}$  of the Nds-IR780 solution ( $2.4\times 10^7$  nanodroplets/mL), IR-780 iodide solution or saline were injected into every nude mouse of group 1, 2, or 3, respectively, through the caudal vein. After 8 h, all of the tumors were irradiated by the photothermal therapy apparatus (1  $\text{w}/\text{cm}^2$ , 210 s), and the distance between the transducer and tumor was approximately 1 cm. At the same time, the local temperature of the tumor was detected by an electronic thermometer and the change before and after the treatment was recorded. Meanwhile, ultrasound imaging was performed on the tumors every two days before and after photothermal therapy, and the tumor volume was calculated by “length $\times$ width $\times$ height $\times\pi/6$ ”. The treatment effect was expressed by  $v/v_0$  (where  $v$ =the tumor volume after treatment, and  $v_0$ = the tumor volume before treatment).

## Statistical methods

Independent-sample  $t$ -tests and analysis of variance (ANOVA) were performed for statistical analyses of all groups. A 95% confidence level was used to determine the significance between groups, and  $P<0.05$  was designated as significant. All data were reported as the mean  $\pm$  standard deviation.

## Results and discussion

CMM, one of the most aggressive skin cancers, has become a leading cause of cancer death in recent years because the incidence rate of the disease has rapidly increased worldwide.<sup>2</sup> The poor prognosis of CMM is mainly

attributed to the difficulty of accurately detecting small melanomas, which may have metastatic potential, and the identification of benign and malignant melanomas through histopathological examination. In recent years, the development of ultrasound molecular imaging and nanomaterial technology has brought new solutions to this problem. Phase-change nanodroplets as ultrasound molecular imaging contrast agents for noninvasive, accurate detection and targeted therapy of tumors have attracted wide attention. In this study, we prepared new targeted phase-change nanodroplets named Nds-IR780 for precise diagnosis and targeted treatment of cutaneous malignant melanoma through a noninvasive strategy.

## Exploration of the appropriate loading amount and biocompatibility of IR-780 iodide in Nds-IR780

First, using HPLC, the standard curve of IR-780 iodide was drawn (Figure 2A). The concentrations of IR-780 iodide in the Nds-IR780 suspensions varied at  $8.6 \pm 0.83 \mu\text{g/ml}$ ,  $20.5 \pm 1.7 \mu\text{g/ml}$  and  $30.2 \pm 1.45 \mu\text{g/ml}$  as the amount of IR-780 iodide increased (50  $\mu\text{g}$ , 100  $\mu\text{g}$ , 150  $\mu\text{g}$ ), the signal of Nds-IR780 at 2 min gradually increased at 780 nm (Figure 2B). Interestingly, as shown in Figure 2C and D, when the amount of IR-780 iodide

increased from 50  $\mu\text{g}$  to 100  $\mu\text{g}$ , the ER obviously increased, and the difference was statistically significant ( $52\% \pm 1.56\%$  vs  $62\% \pm 1.21\%$ ,  $P < 0.05$ ). However, when the amount of IR-780 iodide increased to 150  $\mu\text{g}$ , the ER started to fall; the change was not significantly different ( $62\% \pm 1.21\%$  vs  $60\% \pm 0.8\%$ ,  $P > 0.05$ ). For DL, when the amount of IR-780 iodide increased from 50  $\mu\text{g}$  to 100  $\mu\text{g}$  to 150  $\mu\text{g}$ , the DL increased from  $0.4 \pm 0.08\%$ ,  $0.9 \pm 0.079\%$  to  $1.3 \pm 0.14\%$ , respectively, and the difference between the DL of the 50  $\mu\text{g}$  solution and that of the 150  $\mu\text{g}$  solution was statistically significant ( $P < 0.05$ ). The results indicated that the saturation capacity of IR-780 iodide on the shells of Nds-IR780 is 100  $\mu\text{g}$  but the DL increased even when addition of IR-780 iodide increased to 150  $\mu\text{g}$ . Using 150  $\mu\text{g}$  of IR-780 iodide was more appropriate than using 50  $\mu\text{g}$  and 100  $\mu\text{g}$ . It is worth mentioning that although the DL was low, the quantity of IR-780 iodide on the shells of Nds-IR780 was sufficient for the diagnosis and treatment of tumors, which was verified by our next study.

The biocompatibility of Nds-IR780 was confirmed by the CCK-8 assay. As shown in Figure 2E, when the Nds-IR780 suspension was diluted 10 times and the quantity of IR-780 iodide was 18.2  $\mu\text{g/mL}$ , the cell viability notably decreased, and the difference was statistically significant ( $99 \pm 1.92\%$  vs  $25 \pm 1.26\%$ ,  $P < 0.05$ ). Therefore, the Nds-

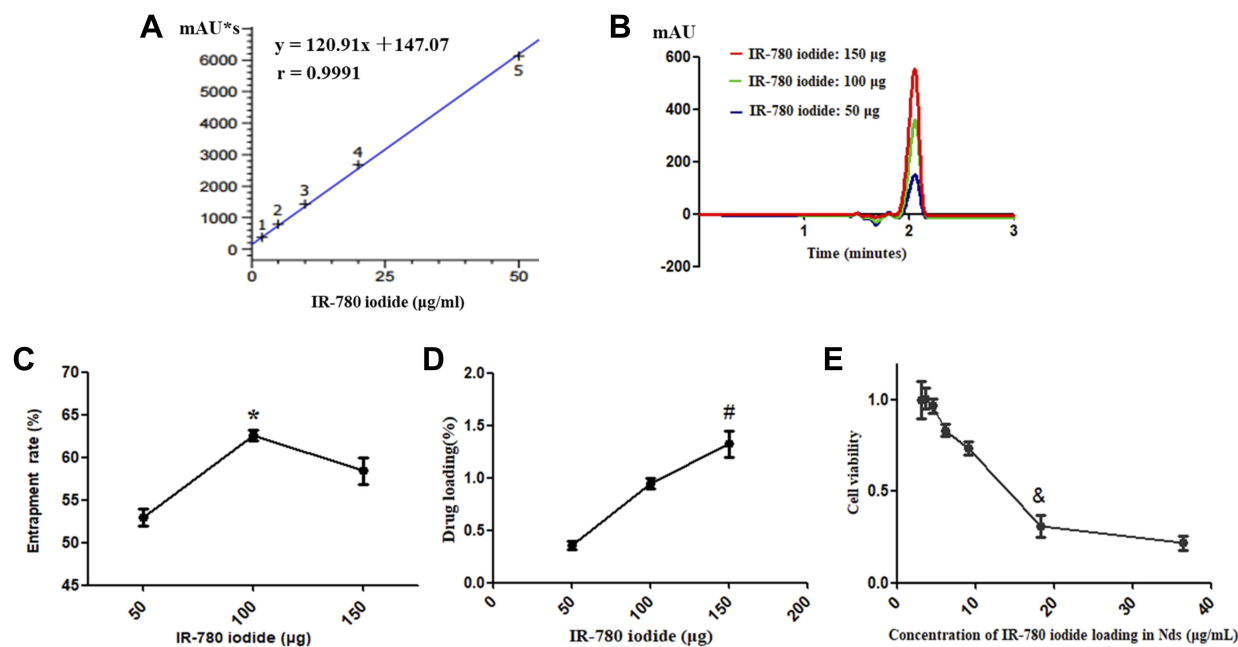


**Figure 2** Exploration of the appropriate loading amount and biocompatibility of IR-780 iodide in Nds-IR780. (A) The standard curve of IR-780 iodide. (B) The signal intensity of Nds-IR780 with different amounts of IR-780 iodide added at 780 nm by HPLC. (C) The ER of IR-780 iodide in Nds-IR780 with different amounts added. \* $P < 0.05$  compared with the ER in the 50  $\mu\text{g}$  added group. (D) The DL of IR-780 iodide in Nds-IR780 with different amounts added. # $P < 0.05$  compared with the DL in the 50  $\mu\text{g}$  added group. (E) The biocompatibility of IR-780 iodide in Nds-IR780. & $P < 0.05$  compared with the cell viability of Nds-IR780 diluted 60 times.

IR780 suspension should be diluted more than 10 times in the next in vivo experiments.

## The preparation of Nds-IR780

As shown in Figure 3, 150  $\mu\text{g}$  of IR-780 iodide was successfully integrated into the shell of the nanodroplets, and the Nds-IR780 solution presented with a homogeneous light green suspension appearance (Figure 3A). Under the CLSM, the nanodroplets showed obvious near infrared fluorescence (Figure 3B), and the results further confirmed that the IR-780 iodide was successfully loaded onto the shell of the nanodroplets. It is well-known that using IR-780 iodide has many advantages, such as being able to facilitate NIRF imaging, which can penetrate up to deep distance, specifically target tumors, facilitate photothermal ablation and create photodynamic effects for

tumors.<sup>16</sup> However, because of its insolubility in water, the clinical application of IR-780 iodide has been greatly limited. Interestingly, we used the liposoluble properties of IR-780 iodide to successfully load it onto the lipid shells of phase-change nanodroplets, which can not only increase the specific targeting ability of the nanodroplets for tumors but can also provide a suitable carrier for IR-780 iodide. Additionally, Nds-IR780 were observed by TEM and exhibited perfect spherical morphology (Figure 3C). Because the PFH core is liquid and the boiling point is approximately 56  $^{\circ}\text{C}$ , Nds-IR780 were stereoscopically round in appearance and stable under TEM at room temperature, unlike previous micro- or nanobubbles.<sup>17–19</sup> The diameter and zeta potential of the Nds-IR780 nanoemulsions were determined by DLS, and the results were  $171.8 \pm 57.6$  nm (Figure 3D) and  $-20.76 \pm 6.9$  mv, respectively.

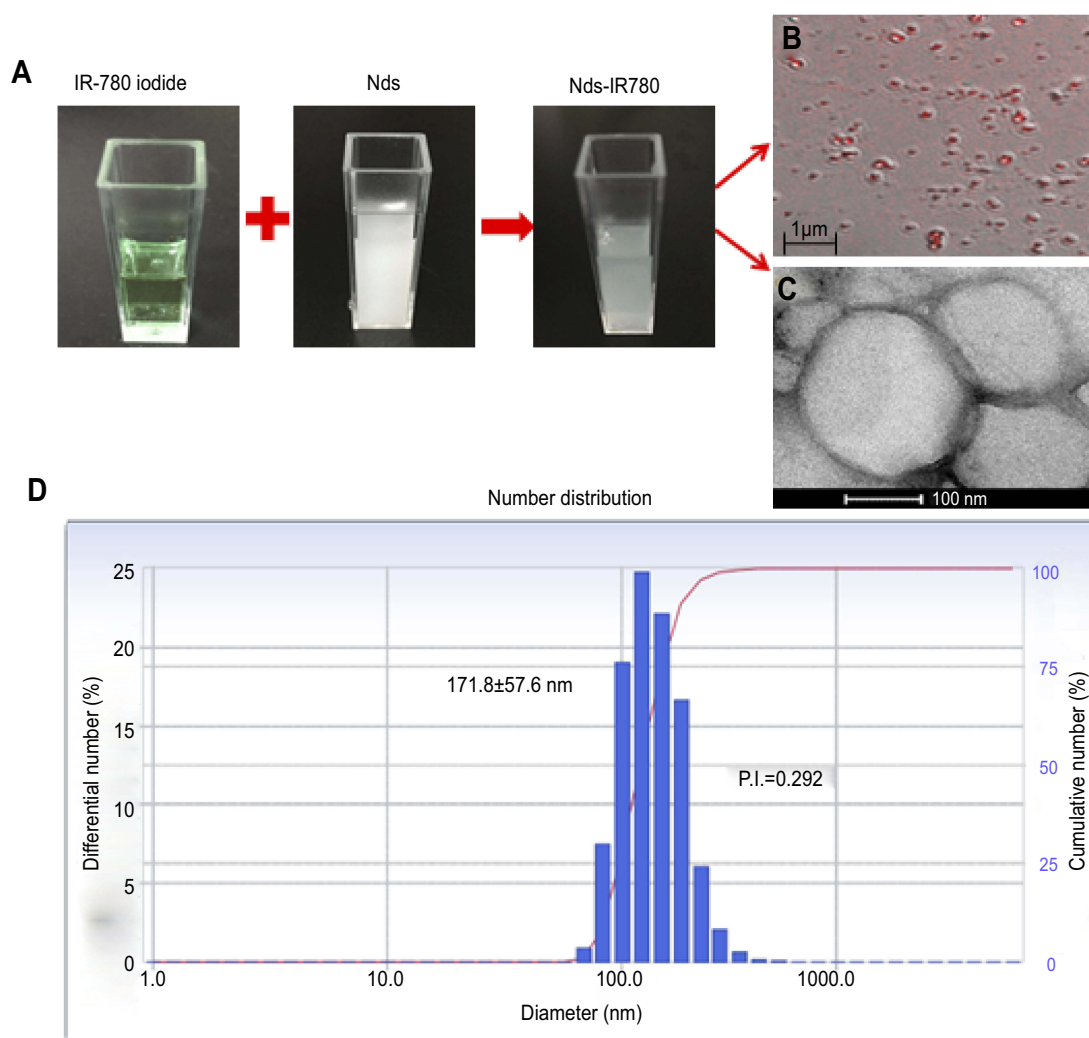


**Figure 3** Characteristics of Nds-IR780. (A) Fabrication of Nds-IR780 observed by the naked eyes. (B) LSCM image of Nds-IR780 with an oil immersion objective lens (100 $\times$ ). (C) TEM image of Nds-IR780. (D) Number distribution of Nds-IR780' size.

Compared with microbubbles, Nds-IR780 are smaller in size, which makes them more conducive to penetrating the vascular leaks of the tumor via the EPR effect. At the same time, the negative potential on the surface of the Nds-IR780 nanoparticles can prevent adhesion and aggregation as the nanodroplets flow in the blood.

### The stability of Nds-IR780

Compared with microbubbles as ultrasound contrast agents, the greatest advantage of phase-change nanodroplets is their good stability.<sup>20</sup> In this study, we verified the stability of Nds-IR780. As shown in Figure 4, the initial size of Nds-IR780 was approximately 200 nm, and the size distribution was  $220\pm 67.2$  nm. After 24 h and 72 h of storage at 4 °C, the size distribution decreased to  $197.9$

$\pm 54.9$  nm and  $171.4\pm 50.2$  nm, respectively. At the same time, the Polydispersity Index (P.I.) decreased from 0.320 at room temperature to 0.239 after 24 h of storage and 0.190 after 72 h of storage. Importantly, there was no significant difference ( $P<0.05$ ) in not only the change in the size distribution but also the change in P.I. When the solution is placed in a static state, the larger particles are more likely to settle down to the bottom, while smaller particles are suspended in the upper layer. In this study, the results were typically attributed to the smaller Nds-IR780 suspended in the upper layer; the gradually decreasing P.I. indicates that the Nds-IR780 size becomes more homogeneous with increasing static time. In our research, after softly shaking the solution, the Nds-IR780 on the bottom will resuspend and the size and P.

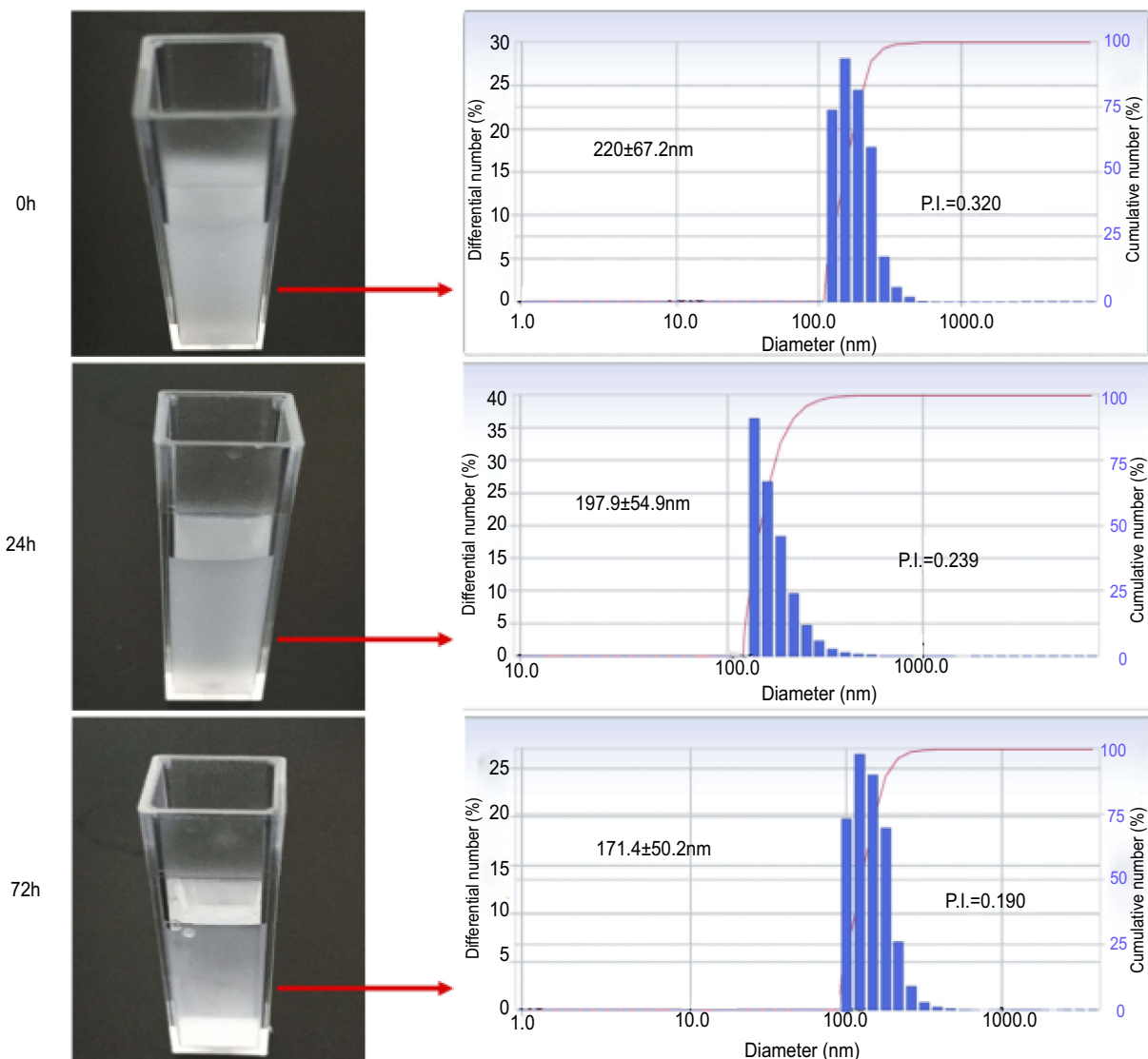


**Figure 4** The stability observation of Nds-IR780 at 0 h, 24 h and 72 h.

I. revert back to the initial state. After 12 days, we found that the size and P.I. of Nds-IR780 had not changed much.

### The dual-mode imaging characteristic of Nds-IR780 in vitro

First, NIRF imaging was performed using different concentrations of Nds-IR780. As shown in Figure 5A, the concentration of Nds-IR780 ranged from high to low (sample 1 to 6), and the results indicated that the NIRF signal was obvious and that the intensity ranged accordingly from high to low based on Nds-IR780 concentration; there was no NIRF in the PBS (sample 7) and control (sample 8). Next, phase change and ultrasound contrast imaging of Nds-IR780 were performed in vitro via homemade equipment. Before the phase change, the Nds-IR780 were subjected to weak ultrasound enhanced imaging, and the nanodroplets appeared

as uniformly small particles with an optical microscope (Figure 5B and C). Normally, liquid fluorocarbon coated with liposome cannot be seen with ultrasound contrast imaging; thus, the weak contrast-enhanced ultrasound signals in this study may be attributed to the interface between the lipid shell membrane and water. Interestingly, after being irradiated for 0 s by low frequency ultrasound, the Nds-IR780 exhibited stronger intensity in ultrasound contrast imaging, and many larger bubbles appeared under the optical microscope (Figure 5D and E).

### The tumor-targeting characteristics of Nds-IR780 in vitro

We cultured the CMM cells SK-MEL-28 and verified the tumor-targeting feature of Nds-IR780 through LSCM, furthermore, the IR-780 iodide absorption in CMM cells was detected via FCM. The results showed that in the Nds-

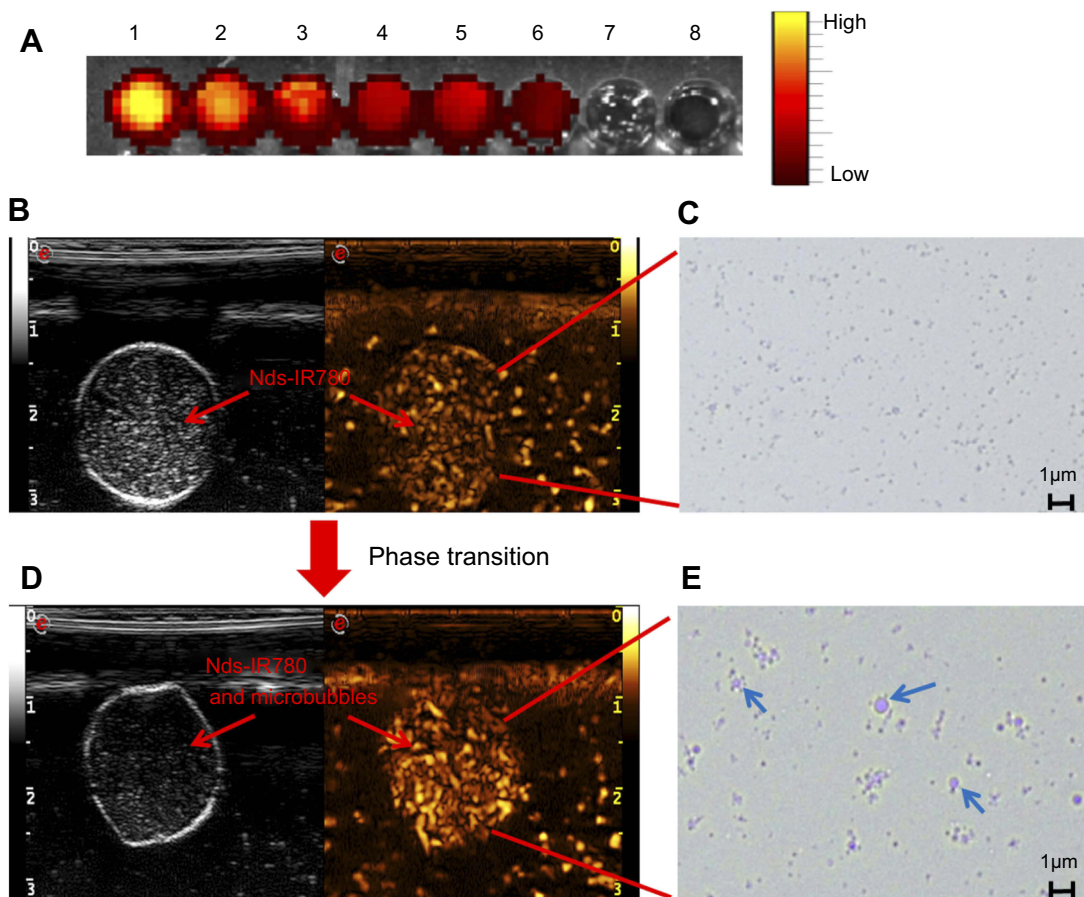


**Figure 5** The dual-mode imaging and phase change ability of Nds-IR780. (A) NIRF imaging of Nds-IR780 (from wells 1 to 7: the Nds-IR780 concentration from high to low; well 8: 1×PBS as control). (B, D) Contrast-enhanced ultrasound imaging before and after Nds-IR780 phase transition in vitro. (C, E) Observation of Nds-IR780 phase transition by Optical Microscope. The blue arrows indicate microbubbles.

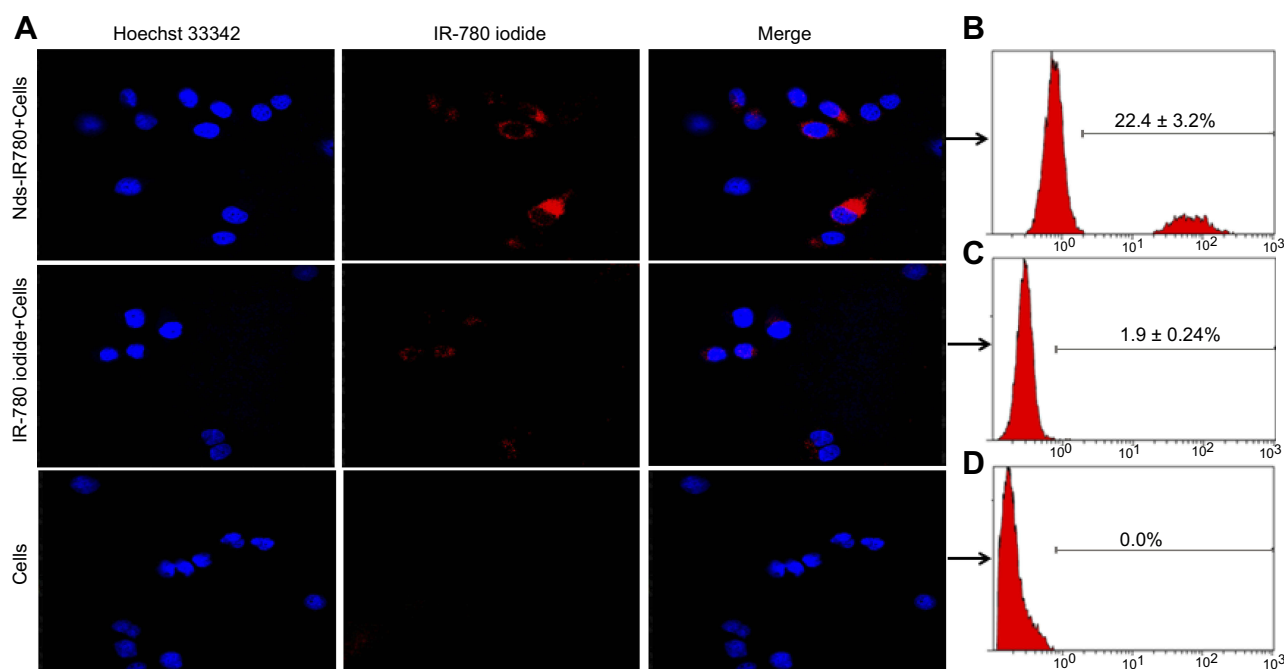


**Figure 6** Tumor-targeting ability of Nds-IR780 was evaluated by co-incubation with SK-MEL-28 cells in vitro. (A) NIRF imaging and merged images of SK-MEL-28 cells incubated with Nds-IR780, IR-780 iodide and PBS. Magnification: 400 $\times$ . The NIRF absorption quantity by SK-MEL-28 cells in Nds-IR780+cells (B), IR-780+cells (C) and PBS +cells (D) via FCM analysis.

IR780+ cells group, there was high NIRF signal in the cancer cells, and the proportion of stained cells was  $22.4 \pm 3.2\%$  (Figure 6A and B). In contrast, in the IR-780 iodide + cells and control groups, there was little or no NIRF signal in the cancer cells (Figure 6A), and the proportions of stained cells were  $1.9 \pm 0.24\%$  and  $0\%$ , respectively (Figure 6A, C and D). Compared with IR-780 iodide, Nds-IR780 were more likely to target the tumor cells, and the difference between the Nds-IR780+ cells group and the IR-780 iodide + cells group was statistically significant ( $P < 0.05$ ). Despite the high affinity of IR-780 iodide for cancer cells, the water-insoluble nature of IR-780 iodide makes it less accessible to cancer cells, which was also verified in this study. Recently, some researchers loaded IR-780 iodide onto nanoparticles and successfully conducted tumor-target therapy.<sup>16,21–23</sup> However, nanoparticles are easily deposited in vivo and cause toxicity. To date, there have been few studies loading IR-780 iodide in lipid nanodroplets as multi-functional ultrasound contrast agents. In this study, the new probe Nds-IR780 may overcome the above deficiencies because the Nds-IR780 that coats the liquid perfluorohexane can be easier to exhale through the lungs after the liquid-gas phase transition, and the lipid shells of Nds-IR780 are recognized as nontoxic to the body.

## The tumor-targeted effect and biodistribution of Nds-IR780 in vivo

As shown in Figure 7, the same amount of saline, IR-780 iodide and Nds-IR780 was respectively injected into the tail vein of nude mice, after 6h, there were lots of fluorescence accumulating in the tumor in Nds-IR780 group but little in that in IR-780 iodide group, meanwhile, there is no fluorescence in saline group. The results indicated that the nanodroplets loaded more IR-780 iodide getting to the tumor compared to the single IR-780 iodide. Although the IR-780 iodide has specific targeting function to most of tumor, its insolubility in water greatly prevents this function from playing its role. The Nds-IR780 have good potential of carrying enough IR-780 iodide to tumor. Moreover, the biodistribution of Nds-IR780 was detected at 1h, 8h and 24h. After 1 h, the NIRF signal was mainly in the liver, lung and kidneys, and there was little fluorescence in the tumor. After 8 h, the tumor was filled with strong NIRF signal, and there was less fluorescence in the liver, lung, kidneys and other organs. Lastly, when the time was prolonged to 24 h, the NIRF signal in the tumor gradually faded away, and the fluorescence was mainly in the liver, lung and kidneys again, whereas there was little fluorescence in the spleen, heart and

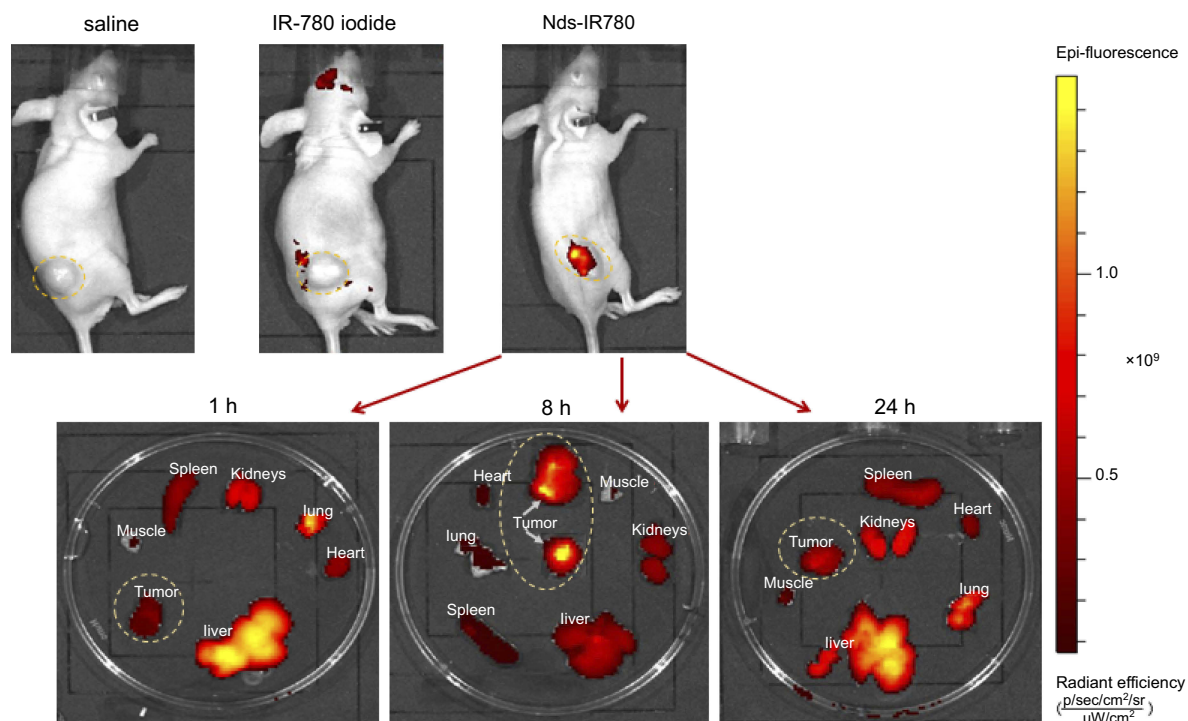


**Figure 7** The in vivo tumor-targeted effect of Nds-IR780 at 6h and biodistribution of Nds-IR780 at 1 h, 8 h and 24 h evaluated by NIRF imaging via an IVIS Lumina II imaging station. The yellow dotted circles indicated the tumors.

muscle. The results indicated that most of the Nds-IR780 accumulated in the tumors in vivo at 8 h after injection. In previous studies,<sup>22</sup> the fluorescence of IR-780 iodide was usually detected in tumors after 24 h via caudal vein injection, but in this study, the nanodroplets loaded with IR-780 iodide shortened the tumor targeting time, which may be attributed to the EPR effect of nanodroplets, and the smaller size helps the nanoparticles avoid being ingested by phagocytes.

### The dual-mode imaging of Nds-IR780 for precise detection of tumors and SLNs in vivo

It is well-known that cutaneous malignant melanoma can easily metastasize early and that micrometastases are not easily detected. In this study, we confirmed that the newly prepared Nds-IR780 could not only detect subcutaneous xenotransplanted melanoma but also detect metastatic SLN through noninvasive dual-mode imaging. As shown in Figure 8, Nds-IR780 were first injected through the caudal vein of nude mice bearing subcutaneous xenotransplanted melanoma (Figure 8A). Then, the tumor was irradiated by low

frequency ultrasound for 20 s. Under contrast-enhanced ultrasound mode, the tumor border was clearly observed (Figure 8B and C). To verify whether Nds-IR780 can detect the micrometastases of melanoma more accurately, NIRF imaging was performed. In Figure 8D, the NIRF signal was obvious in the tumor region but there were no NIRF signals in other organs of the mouse. Interestingly, in the right inguinal region, we also detected NIRF signals, which were lymph node metastases that were later verified by two-dimensional ultrasound (Figure 8E and F). Obviously, the two imaging modes of Nds-IR780 can play a complementary role in detecting small primary and SLNs. In the clinic, precise detection and thorough dissection of metastatic lymph nodes in patients with malignant tumors during operation are very important to improve the prognosis of the patients. At the present, among the various near-infrared agents, only indocyanine green (ICG) is approved by the United States Food and Drug Administration for clinical applications in detecting metastatic lymph nodes; however, ICG has the disadvantages of being unstable in aqueous solution and is quickly cleared in vivo.<sup>24</sup> In this study, the noninvasiveness, stability and dual-mode imaging characteristics of

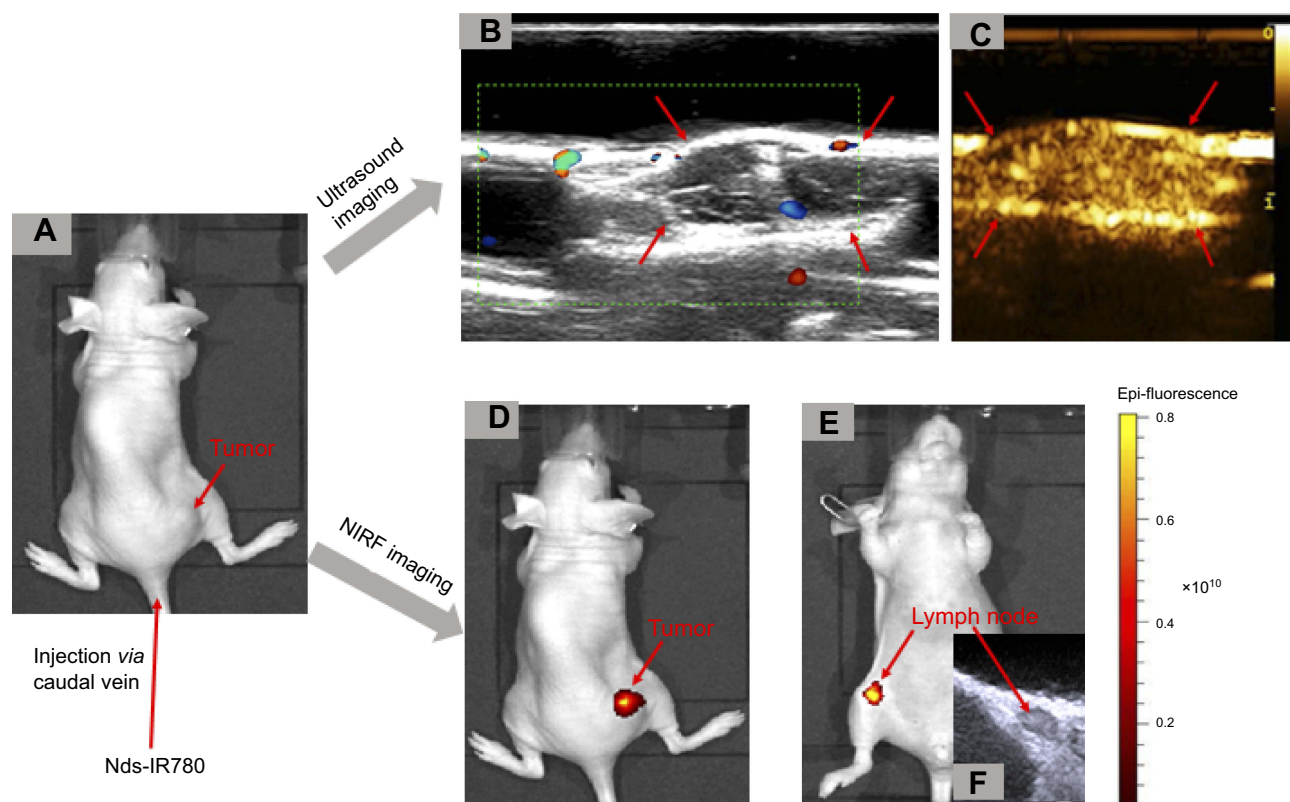


**Figure 8** The detection of CMM by Nds-IR780 through dual-mode imaging in vivo. (A) A nude mouse bearing CMM. (B, C) Color Doppler flow imaging and contrast-enhanced ultrasound imaging after phase transition for CMM by Nds-IR780. (D) NIRF imaging of CMM with Nds-IR780. (E) NIRF imaging of SLNs with Nds-IR780. (F) Two-dimensional ultrasound imaging of SLNs.

Nds-IR780 have been confirmed, which is bound to have potential advantages in the accurate detection of metastatic lymph nodes of CMM.

### Targeted photothermal therapy induced by Nds-IR780 for tumors

According to the results of Nds-IR780 biodistribution in vivo, the targeting photothermal therapy for tumor was performed at 8h after injecting Nds-IR780. In Figure 9A, the subcutaneous xenotransplanted melanomas of different groups were irradiated with an 808 nm laser at  $1 \text{ w/cm}^2$  for 210 s. To observe the photothermal effect induced by Nds-IR780 in the local tumor, the local temperature of the tumor was detected before and after irradiation by the laser. As shown in Figure 10A, in the Nds-IR780 group, the pre-treatment temperature was  $35.4 \pm 1.8 \text{ }^\circ\text{C}$ , and the post-treatment temperature was  $51 \pm 1.2 \text{ }^\circ\text{C}$ . The difference was statistically significant ( $P < 0.05$ ). In contrast, although the IR-780 iodide group had little heating before and

after treatment, the difference was not statistically significant ( $P > 0.05$ ). In the control group, there was little change in temperature. Next, the change in tumor size was monitored via two-dimensional ultrasound imaging for 15 days. The results showed that the tumor disappeared in the Nds-IR780 group at 15 days after treatment. However, in the IR-780 iodide group, although the tumor size decreased 9 days after treatment, there was an increase again in the periphery of the tumor at 15 days after treatment. For the control group, the size of the tumor is constantly increasing to approximately four times the initial size of the tumor (Figure 9B, Figure 10B). The greatest advantage of photothermal therapy is that it can avoid the normal tissue around the lesion and only ablate the area where the photosensitizers are aggregated.<sup>25–28</sup> In this study, the new probe Nds-IR780 had a highly targeted effect on the CMM tumor and its SLNs; the tumor photothermal ablation mediated by Nds-IR780 was also more efficient. Clearly, this noninvasive treatment is more accurate than traditional therapies.

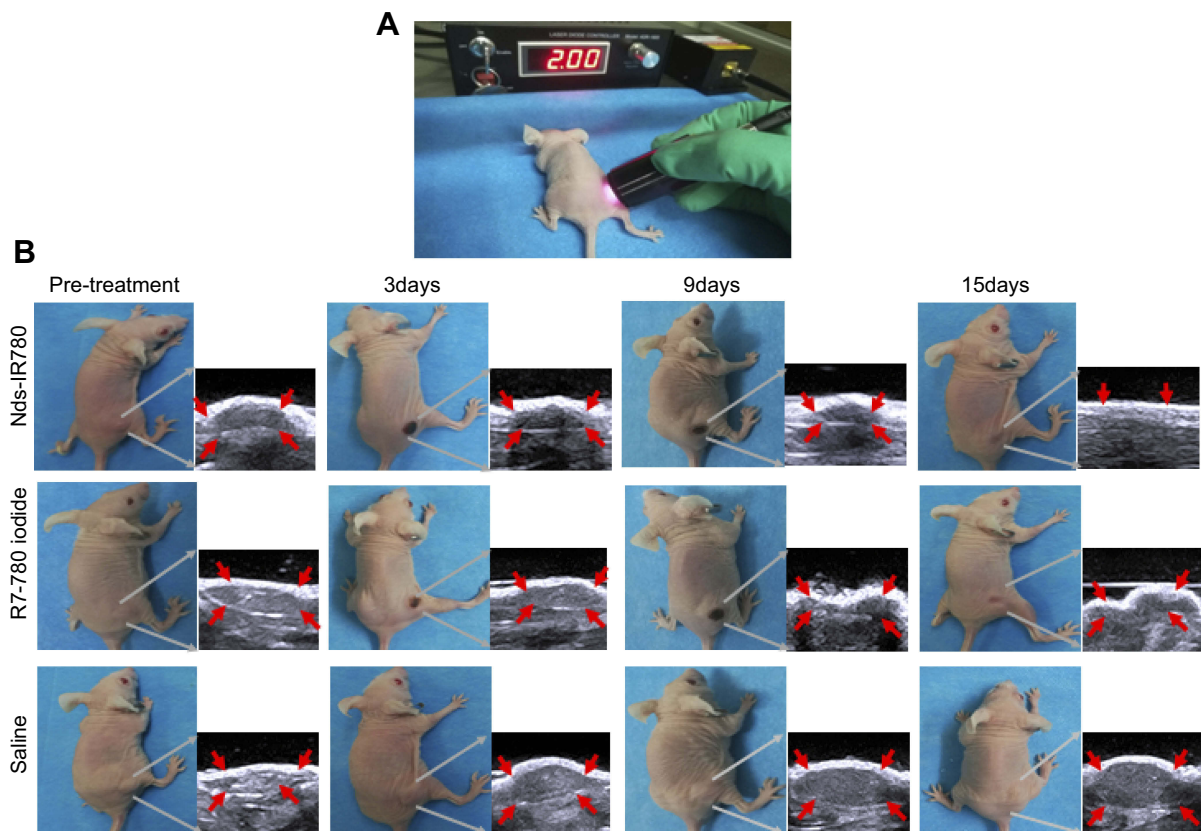


**Figure 9** The photothermal treatment of CMM mediated by Nds-IR780 in vivo. **(A)** The photothermal treatment procedure for CMM by laser at 808 nm. **(B)** Tumor volume monitoring by two-dimensional ultrasound before and after treatment.

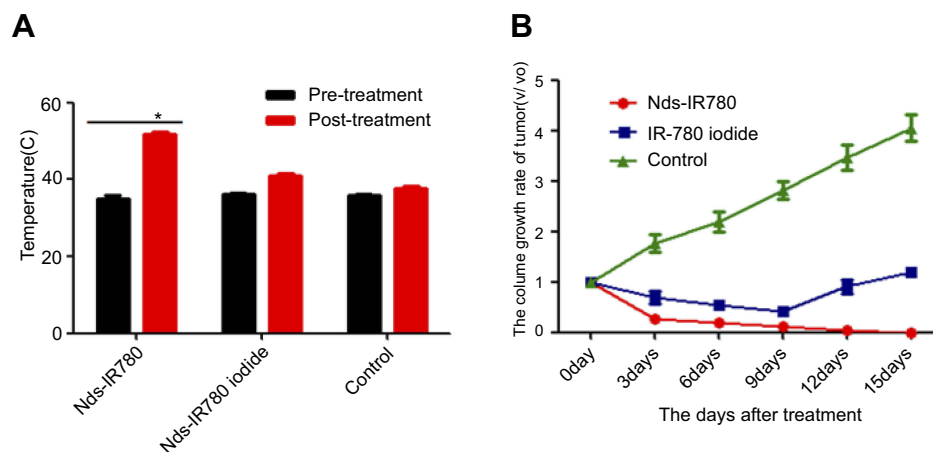


**Figure 10** Temperature changes and tumor volume changes before and after treatment in different groups. **(A)** Temperature changes of tumor surface before and after treatment in the Nds-IR780, IR-780 iodide and control groups. \* $P < 0.05$ , compared with the temperature before treatment in the Nds-IR780 group. **(B)** Comparison of tumor volume growth rate in the Nds-IR780 group, IR-780 group and control group during 15 days.

## Conclusion

The novel probe Nds-IR780 were demonstrated to be good noninvasive theranostic probes, which may provide precise detection for the primary lesions and SLNs of CMM through dual-mode molecular-targeted ultrasound imaging combined with NIRF imaging.

Furthermore, the photothermal ablation of CMM mediated by Nds-IR780 was very effective.

## Acknowledgments

This research was financially supported by the second-class General Financial Grant from the China Postdoctoral Science

Foundation (grant number 2017M613420) and the National Natural Science Foundation of China (grant number 81671706). The authors thank Professor Chih-Kuang Yeh (Department of Biomedical Engineering and Environmental Sciences, National Tsing Hua University, Taiwan) for his assistance. The authors are grateful to the Department of Molecular Biology, Fourth Military Medical University for their kind provisions of equipment and technical support.

## Disclosure

The authors report no conflicts of interest in this work.

## References

- Ankeny JS, Labadie B, Luke J, et al. Review of diagnostic, prognostic, and predictive biomarkers in melanoma. *Clin Exp Metastasis*. 2018;35(5-6):487-493. [PubMed: 29722000]. doi:10.1007/s10585-018-9892-z
- Abbas O, Miller DD, Bhawan J. Cutaneous malignant melanoma: update on diagnostic and prognostic biomarkers. *Am J Dermatopathol*. 2014;36(5):363-379. [PubMed: 24803061]. doi:10.1097/DAD.0b013e31828a2ec5
- Miller KD, Siegel RL, Lin CC, et al. Cancer treatment and survivorship statistics, 2016. *CA Cancer J Clin*. 2016;66(4):271-289. [PubMed: 27253694]. doi:10.3322/caac.21349
- Cai T, Kuang Y, Zhang C, et al. Glucose-6-phosphate dehydrogenase and NADPH oxidase 4 control STAT3 activity in melanoma cells through a pathway involving reactive oxygen species, c-SRC and SHP2. *Am J Cancer Res*. 2015;5(5):1610-1620. [PubMed: 26175932].
- D'Aniello C, Perri F, Scarpati GDV, et al. Melanoma adjuvant treatment: current insight and clinical features. *Curr Cancer Drug Targets*. 2018; 18(5):442-456. [PubMed: 28183255]. doi:10.2174/1568009617666170208163714
- Cabrera R, Recule F. Unusual Clinical Presentations of Malignant Melanoma: a Review of Clinical and Histologic Features with Special Emphasis on Dermatologic Findings. *Am J Clin Dermatol*. 2018;19 (Suppl 1):15-23. [PubMed: 30374898]. doi:10.1007/s40257-018-0373-6
- Houghton JL, Zeglis BM, Abdel-Atti D, et al. Site-specifically labeled CA19.9-targeted immunconjugates for the PET, NIRF, and multimodal PET/NIRF imaging of pancreatic cancer. *Proc Natl Acad Sci U S A*. 2015;112(52):15850-15855. [PubMed: 26668398]. doi:10.1073/pnas.1506542112
- Luo MH, Yeh CK, Situ B, Yu JS, Li BC, Chen ZY. Microbubbles: a Novel Strategy for Chemotherapy. *Curr Pharm Des*. 2017;23(23):3383-3390. [PubMed: 28088911]. doi:10.2174/1381612823666170113092148
- Kripfgans OD, Fowlkes JB, Miller DL, Eldevik OP, Carson PL. Acoustic droplet vaporization for therapeutic and diagnostic applications. *Ultrasound Med Biol*. 2000;26(7):1177-1189. [PubMed: 11053753]. doi:10.1016/S0301-5629(00)00262-3
- Rapoport N, Nam KH, Gupta R, et al. Ultrasound-mediated tumor imaging and nanotherapy using drug loaded, block copolymer stabilized perfluorocarbon nanoemulsions. *J Control Release*. 2011; 153 (1):4-15. [PubMed: 21277919]. doi:10.1016/j.jconrel.2011.01.022
- Sheeran PS, Rojas JD, Puett C, Hjelmquist J, Arena CB, Dayton PA. Contrast-enhanced ultrasound imaging and in vivo circulatory kinetics with low-boiling-point nanoscale phase-change perfluorocarbon agents. *Ultrasound Med Biol*. 2015;41(3):814-831. [PubMed: 25619781]. doi:10.1016/j.ultrasmedbio.2014.10.020
- Deng L, Cai X, Sheng D, et al. A laser-activated biocompatible theranostic nanoagent for targeted multimodal imaging and photothermal therapy. *Theranostics*. 2017; 7(18):4410-4423. [PubMed: 29158836]. doi:10.7150/thno.21283
- Yi X, Yan F, Wang F, et al. IR-780 dye for near-infrared fluorescence imaging in prostate cancer. *Med Sci Monit*. 2015;21:511-517. [PubMed: 25686161]. doi:10.12659/MSM.892437
- Svoboda M, Riha J, Wlcek K, Jaeger W, Thalhammer T. Organic anion transporting polypeptides (OATPs): regulation of expression and function. *Curr Drug Metab*. 2011;12(2):139-153. [PubMed: 21395542].
- Green SM, Kaipainen A, Bullock K, et al. Role of OATP transporters in steroid uptake by prostate cancer cells in vivo. *Prostate Cancer Prostatic Dis*. 2017;20(1):20-27. [PubMed: 27645128]. doi:10.1038/pcan.2016.42
- Pais-Silva C, de Melo-Diogo D, Correia IJ. IR780-loaded TPGS-TOS micelles for breast cancer photodynamic therapy. *Eur J Pharm Biopharm*. 2017;113:108-117. [PubMed: 28087376]. doi:10.1016/j.ejpb.2017.01.002
- Yang H, Cai W, Xu L, et al. Nanobubble-affibody: novel ultrasound contrast agents for targeted molecular ultrasound imaging of tumor. *Biomaterials*. 2015;37:279-288. [PubMed: 25453958]. doi:10.1016/j.biomaterials.2014.10.013
- Cai WB, Yang HL, Zhang J, et al. The optimized fabrication of nanobubbles as ultrasound contrast agents for tumor imaging. *Sci Rep*. 2015;5:13725. [PubMed: 26333917]. doi:10.1038/srep13725
- Yang H, Zhou T, Cai W, et al. Novel dual-mode nanobubbles as potential targeted contrast agents for female tumors exploration. *Tumour Biol*. 2016; 37(10):14153-14163. [PubMed: 27539728]. doi:10.1007/s13277-016-5238-0
- Lin S, Shah A, Hernandez-Gil J, et al. Optically and acoustically triggerable sub-micron phase-change contrast agents for enhanced photoacoustic and ultrasound imaging. *Photoacoustics*. 2017;6:26-36. [PubMed: 28507898]. doi:10.1016/j.pacs.2017.04.001
- Alves CG, Lima-Sousa R, de Melo-Diogo D, Louro RO, Correia IJ. IR780 based nanomaterials for cancer imaging and photothermal, photodynamic and combinatorial therapies. *Int J Pharm*. 2018;542(1-2):164-175. [PubMed: 29549013]. doi:10.1016/j.ijpharm.2018.03.020
- Shirata C, Kaneko J, Inagaki Y, et al. Near-infrared photothermal/photodynamic therapy with indocyanine green induces apoptosis of hepatocellular carcinoma cells through oxidative stress. *Sci Rep*. 2017; 7(1):13958. [PubMed: 29066756]. doi:10.1038/s41598-017-14401-0
- Deng G, Li S, Sun Z, et al. Near-infrared fluorescence imaging in the largely unexplored window of 900-1,000 nm. *Theranostics*. 2018; 8 (15):4116-4128. [PubMed: 30128040]. doi:10.7150/thno.26539
- Sneddon D, Poulsen SA. Agents described in the molecular imaging and contrast agent database for imaging carbonic anhydrase IX expression. *J Enzyme Inhib Med Chem*. 2014;29(5):753-763. doi:10.3109/14756366.2013.848205
- Hu JJ, Cheng YJ, Zhang XZ. Recent advances in nanomaterials for enhanced photothermal therapy of tumors. *Nanoscale*. 2018;10(48):22657-22672. [PubMed: 30500042]. doi:10.1039/c8nr07627h
- Jiang Y, Li J, Zhen X, Xie C, Pu K. Dual-peak absorbing semiconducting copolymer nanoparticles for first and second near-infrared window photothermal therapy: a comparative study. *Adv Mater*. 2018;30(14):e1705980. [PubMed: 29457284]. doi:10.1002/adma.v30.14
- Wang Y, Cai D, Wu H, et al. Functionalized Cu<sub>3</sub>BiS<sub>3</sub> nanoparticles for dual-modal imaging and targeted photothermal/photodynamic therapy. *Nanoscale*. 2018;10(9):4452-4462. [PubMed: 29451575]. doi:10.1039/c7nr07458a
- Guo Z, Zou Y, He H, et al. Bifunctional platinumed nanoparticles for photoinduced tumor ablation. *Adv Mater*. 2016; 28(46):10155-10164. [PubMed: 27714878]. doi:10.1002/adma.201602738

**International Journal of Nanomedicine**

Dovepress

**Publish your work in this journal**

The International Journal of Nanomedicine is an international, peer-reviewed journal focusing on the application of nanotechnology in diagnostics, therapeutics, and drug delivery systems throughout the biomedical field. This journal is indexed on PubMed Central, MedLine, CAS, SciSearch<sup>®</sup>, Current Contents<sup>®</sup>/Clinical Medicine,

Journal Citation Reports/Science Edition, EMBase, Scopus and the Elsevier Bibliographic databases. The manuscript management system is completely online and includes a very quick and fair peer-review system, which is all easy to use. Visit <http://www.dovepress.com/testimonials.php> to read real quotes from published authors.

Submit your manuscript here: <https://www.dovepress.com/international-journal-of-nanomedicine-journal>